ELSEVIER

Radiotherapy and Oncology 66 (2003) 203–216

RADIOTHERAPY & ONCOLOGY
JOURNAL OF THE EUROPEAN SOCIETY FOR THERAPEUTIC RADIOLOGY AND ONCOLOGY

www.elsevier.com/locate/radonline

Radiotherapy treatment planning of prostate cancer using magnetic resonance imaging alone

Young K. Lee[a,*], Marc Bollet[b], Geoffrey Charles-Edwards[a], Maggie A. Flower[a], Martin O. Leach[c], Helen McNair[d], Elizabeth Moore[c], Carl Rowbottom[e], Steve Webb[a]

[a] *Joint Department of Physics, Institute of Cancer Research and Royal Marsden NHS Trust, Downs Road, Sutton, Surrey SM2 5PT, UK*
[b] *Academic Unit of Radiotherapy and Oncology, Institute of Cancer Research and Royal Marsden NHS Trust, Downs Road, Sutton, Surrey SM2 5PT, UK*
[c] *CRC Clinical Magnetic Resonance Research Group, Institute of Cancer Research and Royal Marsden NHS Trust, Downs Road, Sutton, Surrey SM2 5PT, UK*
[d] *Department of Radiotherapy, Institute of Cancer Research and Royal Marsden NHS Trust, Downs Road, Sutton, Surrey SM2 5PT, UK*
[e] *North Western Medical Physics, Christie Hospital NHS Trust, Wilmslow Road, Manchester M20 4BX, UK*

Received 23 April 2002; received in revised form 11 November 2002; accepted 16 December 2002

Abstract

Purpose: Accurate anatomical delineation of the gross tumour volume (GTV) is crucial for effective radiotherapy (RT) treatment of prostate cancers. Although reference to pelvic magnetic resonance (MR) for improved delineation of the prostate is a regular practice in some clinics, MR has not replaced CT due to its geometrical distortions and lack of electron-density information. The possibility and practicality of using MR only for RT treatment planning were studied.

Materials and methods: The addition of electron-density information to MR images for conformal radiotherapy (CRT) planning of the prostate was quantified by comparing dose distributions created on the homogeneous density- and bulk-density assigned images to original CT for four patients. To quantify the MR geometrical distortions measurements of a phantom imaged in CT (Siemens Somatom Plus 4) and FLASH 3D T1-weighted MR (1.5 T whole body Siemens Magnetom Vision) were compared. Dose statistics from CRT treatment plans made on CT and MR for five patient data were compared to determine if MR-only treatment plans can be made.

Results: The differences between dose-plans on bulk-density assigned images when compared to CT were less than 2% when water and bone values were assigned. Dose differences greater than 2% were observed when images of homogeneous-density assignment were compared to the CT. Phantom measurements showed that the distortions in the FLASH 3D T1-weighted MR averaged 2 mm in the volume of interest for prostate RT planning. For the CT and MR prostate planning study, doses delivered to the planning target volume (PTV) in CT and MR were always inside a 93–107% dose range normalised to the isocentre. Also, the doses to the organs-at-risk in the MR images were similar to the doses delivered to the volumes in the registered CT image when the organ volumes between the two images were similar.

Conclusions: Negligible differences were observed in dose distribution between CRT plans using bone + water CT number bulk-assigned image and original CT. Also, the MR distortions were reduced to negligible amounts using large bandwidth MR sequence for prostate CRT planning. MR treatment planning was demonstrated using a large bandwidth sequence and bulk-assigned images. The development of higher quality, low distortion MR sequence will allow regular practice of this technique.

Keywords: Radiotherapy treatment planning; Prostate cancer; Magnetic resonance imaging; Conformal radiotherapy; Electron-density bulk-assignment

1. Introduction

Prostate cancer is the second most common cancer among the male population in the UK after lung cancer. Over 20 000 new prostate cancer cases in the UK and an estimated 134 000 new cases in the EU are seen each year [3,5]. The treatment of localised prostate cancer is variable and the value of radical curative treatments remains controversial. Nevertheless, it is particularly important to minimise the side effects of treatments in this population of patients with a long life expectancy and to reduce any negative impact on quality of life. Therefore, it is desirable to reduce dose to organs-at-risk (OARs) such as the rectum and bladder whilst treating the prostate with the prescribed dose in radiotherapy treatment of prostate cancer.

The gross tumour volume (GTV) for prostate cancer with low risk of seminal vesicle involvement includes the prostate and base of the seminal vesicles. Delineation of the GTV is crucial for the successful treatment of prostate cancer. Accurate outlining of the GTV is difficult using computed tomography (CT) data due to its limited soft-tissue contrast. Results

* Corresponding author.

0167-8140/03/$ - see front matter © 2003 Elsevier Science Ireland Ltd. All rights reserved.
doi:10.1016/S0167-8140(02)00440-1

from a multi-centre quality assurance exercise by Seddon et al. showed high inter-observer variability in outlining the prostatic apex, the superior aspect of the prostate projecting into the bladder and the base of seminal vesicles [19]. Fiorino et al. found a range of average intra-observer variability to be 1.5–9% and inter-observer variability to be 10–18% for the prostate volumes outlined by five observers on six CTs [6]. These studies demonstrate that the target volume definition is a 'weak link' in the radiotherapy planning and delivery process for prostate cancer. What's more, the correct definition of target volume becomes increasingly important with more sophisticated conformal treatments.

It has become regular practice in some hospitals to refer to magnetic resonance (MR) imaging to aid in diagnosing and staging the tumour and outlining the (GTV) for therapy. The advantage of using MR is that it has higher soft-tissue contrast than does CT, due to its dependence on different contrast mechanisms, and that the relative contrast of tissues can be varied. Studies have revealed that there are significant differences in prostate volumes estimated from MR and CT data. Roach et al. have shown that the GTVs delineated on CT images without contrast were 32% larger than those delineated on T1-weighted (repetition time TR = 600 ms and echo time TE = 12 ms) and T2-weighted fast spin echo (TR = 4000 ms, TE = 104 ms) MR scans for 10 prostate cancer patients [17]. The largest discrepancy averaging 7 mm (range 2–12 mm) between CT and MR was observed in the posterior region of the prostate. The prostatic apex was found to have the second largest discrepancy, averaging 4.5 mm (range 2–12 mm). A more recent study by Rasch et al. concluded, using data for 18 patients, that the ratios of CT- to axial-MR-derived volumes was 1.4 (S.D. ± 0.26) and CT- to coronal-MR-derived prostate volumes was 1.5 (S.D. ± 0.3)[16]. They also found that the CT-derived prostate was 8 mm (S.D. ± 6 mm) larger at the base of the seminal vesicles and 6 mm (S.D. ± 4 mm) larger at the apex of the prostate than the axial-MR derived volumes. Debois et al. showed, using data from 10 patients and three observers, that the inter-observer variation of the prostatic apex location was largest on CT, ranging from 0.54 to 1.07 cm, and smallest on coronal MR, ranging from 0.17 to 0.25 cm [4].

Despite the reduced inter- and intra-observer variability in MR, CT remains the main modality for treatment planning because of a lack of correlation between MR voxel intensities and electron-density information. CT numbers are related to electron density values that are used in treatment planning to calculate dose to the patient and also to correct for variations in tissue inhomogeneity by the calculation of a correction factor. Furthermore, in MR, there may be geometrical distortion due to magnetic field inhomogeneities, gradient non-linearities, susceptibility effects and chemical shifts. Though the distortions observed in the centre of the field-of-view (FOV) tend to be low in most MR sequences, they increase with radial distance from the centre. Distortions of up to 15.0 mm have been recorded by Mizowaki et al. in areas more than 120 mm from the imaging centre using T1-weighted image (TR = 500 ms, TE = 20 ms) and T2-weighted image (TR = 3000 ms, TE = 120 ms)[12]. Though Mizowaki et al. attempt to quantify the reproducibility of geometric distortion in MR for the use in RT treatment planning, this study uses a grid acrylic phantom imaged in a 0.2-T magnet. A commonly used magnetic field for patient studies is 1.5 T and the interfaces between tissue inhomogeneity is expected to cause greater geometrical distortion [1,4,10].

In radiotherapy of brain tumours, MRI has been deemed the imaging modality of choice due to its superior soft-tissue contrast. In a study by Gademann et al., the lack of electron-density information from MRI was shown not to cause discrepancies because the dose distribution was not significantly altered by tissue inhomogeneities in the brain [7]. For prostate RT planning with megavoltage X-rays, where pelvic bone constitutes a large part of the volume irradiated, it cannot be assumed that the dose distribution is unaltered by the inhomogeneity of tissues in the pelvic region and the dose distribution differences need to be quantified. A pilot study by Beavis et al. reported on brain tumour RT plans using homogeneous electron-density assigned to MR images [1]. They concluded in their study that geometric distortions could be minimised in the skull. They achieved this by using a relatively small field-of-view (FOV), an increased receiver bandwidth, and a fast spin-echo acquisition sequence for the brain. Compared to the brain, a larger FOV is required for the pelvis and larger distortions are observed in the outer parts of the FOV. Patient-induced distortions arise as a result of magnetic susceptibility and chemical shift effects.

Despite MR's superior soft-tissue contrast, it has not replaced CT for prostate RT treatment planning due to the lack of electron-density information and geometric distortions caused by magnetic inhomogeneities, non-linear gradients, susceptibility and chemical shifts. By using a combination of both CT and MR to guide planning of radiotherapy treatment of prostate cancer, the time and cost of imaging the patients would increase compared to that of using a single imaging modality (MR). Therefore, the benefit in using one superior imaging modality must be quantified. In this work the effect of treatment planning with MR alone was studied: (i) by testing bulk-assignment of CT numbers in the pelvic area; (ii) by quantifying distortions for a large-bandwidth imaging sequence on a 3D body phantom; and (iii) by creating and comparing treatment plans on CT and MR of the prostate cancer patients. The feasibility of using MR alone for use in conformal RT treatment planning of prostate cancer was determined.

2. Materials and methods

2.1. Validity of CT number bulk-assignment

There is no simple correlation between MR intensities

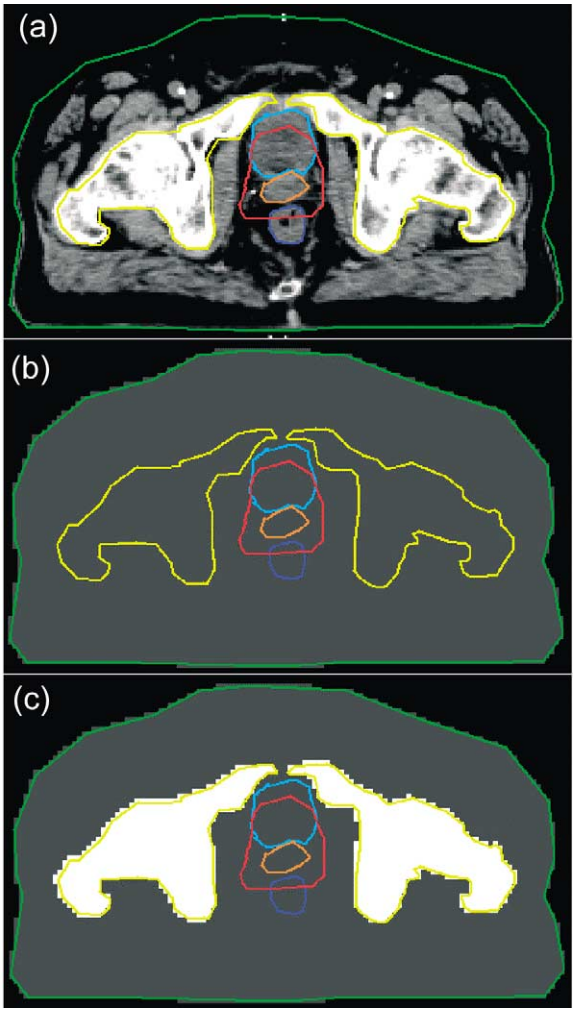

Fig. 1. Corresponding slices of (a) CT, (b) water and (c) bone + water bulk-assigned images. The bulk-assigned values used were equivalent to water and average bone value found from four patients. Orange, red, dark blue and light blue outlines are GTV, PTV, rectum and bladder, respectively. Yellow and green outlines are of bone and patient outline. The margin on the GTV appears larger than 1 cm due to the 3D uniform margin growth from the slice inferior to the slice shown here.

and CT numbers. To create treatment plans on MR, this information must be assigned. The feasibility of assigning CT numbers to MR images, and how this affects the dose distributions, was studied.

Contiguous axial CT scans of four patients with stage T1b/c or T2a prostate cancer were acquired using a Siemens Somatom Plus 4 (Siemens Medical Systems, Erlangen, Germany) with an image matrix size and slice thickness of 256×256 and 5.0 mm. The pixel size ranged from 1.63 to 1.96 mm. The GTVs (prostate and the base of seminal vesicles) and OARs (rectum and bladder) were contoured by a radiotherapy oncologist. The GTV and clinical target volume (CTV) were considered equivalent for prostate cancer treatment. The planning target volume (PTV) included the GTV plus a 1-cm uniform 3D margin. This was in the boundaries of the patient set-up measurements according to Nutting et al. and the margins defined by van Herk et al. and McKenzie et al. [11,13,21].

Using the outlines obtained from the CT image, CT numbers, calculated from electron-density values were assigned in two different ways. Firstly, as shown in Fig. 1b, the body was assumed to be homogeneous, i.e. all the voxels in the body outline were assigned the CT number of water. An electron-density value of $n_0 = 3.340 \times 10^{29}$ m^{-3} (ICRU Report 46 [9]) is set to 0 HU. The new image data will be referred to as I_{water} and individual dose voxel values will be referred to as D_{water}.

Secondly, a bone + water bulk-assigned image was created as follows. The whole bone was manually outlined on the pelvic region for each CT scan. The average value of the four patients' bone CT numbers was found to be 320 HU (range 270–370 HU), equivalent to electron-density value $n_0 = 3.874 \times 10^{29}\text{m}^{-3}$, which is similar to the ICRU value for whole femur, $3.950 \times 10^{29}\text{m}^{-3}$ (365 HU in VOXELPLAN). The average bone value was then assigned to the voxels in the bone outlines. The rest of the voxels in the body were assigned to the water value. This image, as shown in Fig. 1c, will be referred to as $I_{\text{bone+water}}$ and the individual dose voxel values as $D_{\text{bone+water}}$. The average bone-electron-density-equivalent value of 320 HU was used instead of the electron-density-equivalent values given in the ICRU 46 because the large range of bone electron-density values would require segmenting the bone outline into different components of bone (cortical bone and bone marrow). This was not possible since bone cannot be segmented reliably based on contrast of the images.

Conformal RT treatment was planned on the two density-assigned images (I_{water} and $I_{\text{bone+water}}$) and the original CT from which I_{water} and $I_{\text{bone+water}}$ were derived. These three plans that are to be compared will be referred to as I_{water} plan and $I_{\text{bone+water}}$ plan, CT plan. VIRTUOS (VOXELPLAN) treatment planning system was used to plan the CRT treatment with a prescription dose of 64 Gy to be delivered to the PTV using three-irregular-fields, one anterior and two wedged lateral beams with angles 0, 90 and 270°, respectively. A 6-mm field margin was used to account for the dosimetric penumbra of the fields. The beamweights of the fields were kept the same for all three plans. Dose distributions were calculated using a pencil-beam algorithm by Bortfeld et al. with the matrix and pixel sizes 128×128 and 3.9 mm, respectively [2]. This dose distribution, determined using the CT data, was assumed to be the best estimate of the delivered dose distribution.

Dose distribution comparisons between the two density-assigned images (I_{water} and $I_{\text{bone+water}}$) and original CT were made using the following methods.

Test 1: the root mean square difference (rms), in Gy, was calculated for voxels inside known isodose regions of the CT plan as shown in Eq. (1):

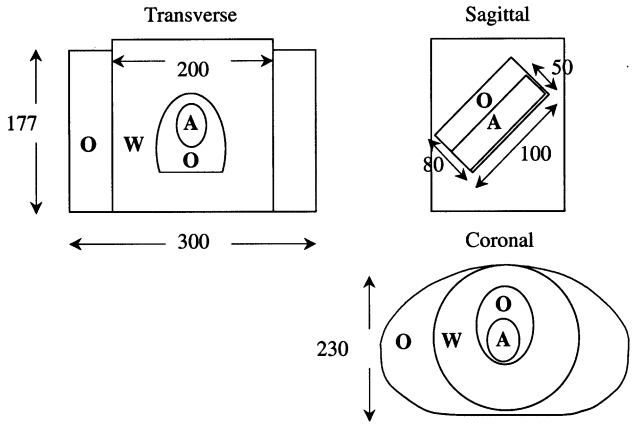

Fig. 2. SPECT/PET Emission Phantom (PTW-Freiburg, Germany) dimensions (in mm) and orientations imaged in CT and MR for distortion measurements (clockwise from left: transverse, sagittal, coronal). The small cylindrical phantom was placed inside the large cylindrical phantom, which was then placed inside the irregular shaped body phantom. The small cylindrical phantom was filled with air (A) and vegetable oil (O) as shown. The large cylindrical phantom was filled with water (W) and the rest of the body phantom was filled with oil.

$$\mathrm{rms}_{(D_{\mathrm{CT}}-D_x)} = \sqrt{\frac{\sum_{i=1}^{n}\left(D_{\mathrm{CT}_i} - D_{x_i}\right)^2}{n}} \quad (1)$$

where D_{CT_i} is the dose in voxel i from the CT plan, D_{x_i} is the dose in voxel i using the bulk-assigned image plans, either D_{water} or $D_{\mathrm{bone+water}}$. The number of voxels in the region studied is represented by n.

Test 2: colour topographical maps were made by displaying the percent difference (Eq. 2) of dose from corresponding voxels from the CT and bulk-assigned plans. This map allowed spatial assessment of the difference in dose distributions.

$$\%\mathrm{diff}_{(D_{\mathrm{CT}}-D_x)_i} = \frac{D_{\mathrm{CT}_i} - D_{x_i}}{D_{\mathrm{CT_i}}} \times 100 \quad (2)$$

The percent difference topographical map was created for all the slices of each of the four patient data sets. The map matrix size was 128×128, the same as the dose matrix size. Percent difference values above a difference of 2% were all depicted with one colour since ICRU Report 42 states that less than 2% difference in dose is considered suitable for radiotherapy treatment planning [8].

2.2. Quantification of MR distortion

MR images are known to contain geometrical distortions. However, effects of the MR distortions are not uniform throughout the image and change with different sequences used. The distortions were quantified by measuring and comparing a large bandwidth sequence MR image of a phantom to a CT image of the phantom.

Different components of a SPECT/PET Emission Phantom (PTW-Freiburg, Germany) were filled with substances to simulate the pelvis. The main body of the pelvis was simulated by the asymmetrical three-dimensional body phantom with a width and height similar to that of the pelvic region imaged for prostate cancer treatment. A schematic of the phantom with its dimensions is shown in Fig. 2. The compartments were filled with air (A), water (W) and vegetable oil (O) as shown in the figure. The phantom is made up of Perspex of 3-mm thickness and rubber and plastic stopper rings.

The phantom was imaged in CT (Fig. 3a) and MR using the FLASH 3D sequence (fast low angle shot), with TR 18.8 ms, TE 5 ms and bandwidth of 244 Hz/pixel (Fig. 3b). This sequence was described by Khoo et al. as providing the best visualisation of the prostate[10]. It was used in conjunction with a large receiver bandwidth to minimise the effects of chemical shift artefacts. This technique employs phase encoding in two of the three dimensions. Distortion in the phase encoding direction is not influenced by the effects of magnetic field inhomogeneity. Thus, in addition to the advantages of acquiring a continuous volume of data, which can be reformatted in any plane similarly to CT, 3D imaging also reduces the amount of distortion due to B-field inhomogeneity.

Bone was not simulated in the phantom since distortion at bone/air interfaces are similar to that of water/air. The phantom was positioned using a reference frame and lasers. The matrix size and slice thickness of the contiguous slices were 256×256 and 5 mm, respectively. Images of 28 slices of the phantom were taken for both CT and MR and were acquired using the Siemens Somatom Plus 4 CT scanner and 1.5-T whole body Siemens Magnetom Vision (Siemens Medical Systems, Erlangen, Germany), respectively.

Voxel intensities were plotted along the x-axis through the centre ($y = 128$) and at approximately 10 cm from the centre of the image ($y = 78$ and 178). Voxel intensities were also plotted along the y-axis through the centre ($x = 128$), at 10 ($x = 78$ and 178) and 14 cm ($x = 58$ and 198) from the centre of the image as shown in Fig. 3. The voxel intensity was plotted for the central slice and slices located 35 and 70 mm superior and inferior to the central slice. The shapes of the voxel intensity curves were visually compared and the distances between the lettered positions from MR and CT were measured to an accuracy of 0.5 voxel (0.9 mm). The edges of intensities were determined from the midpoint of the slopes from the voxel intensity plots. The distances measured by CT were seen as the 'gold standard'.

2.3. CT vs. MR prostate treatment planning

To illustrate that conformal radiotherapy treatment plans can be made using only MR, comparison was made between treatment plans made using CT only and treatment plans using MR only.

Five patients with localised prostate cancer who were to be treated with radical RT were selected for this study. Two patients were diagnosed with stage T1c, two were diagnosed stage T2a and one was diagnosed stage T2b. The CT scans

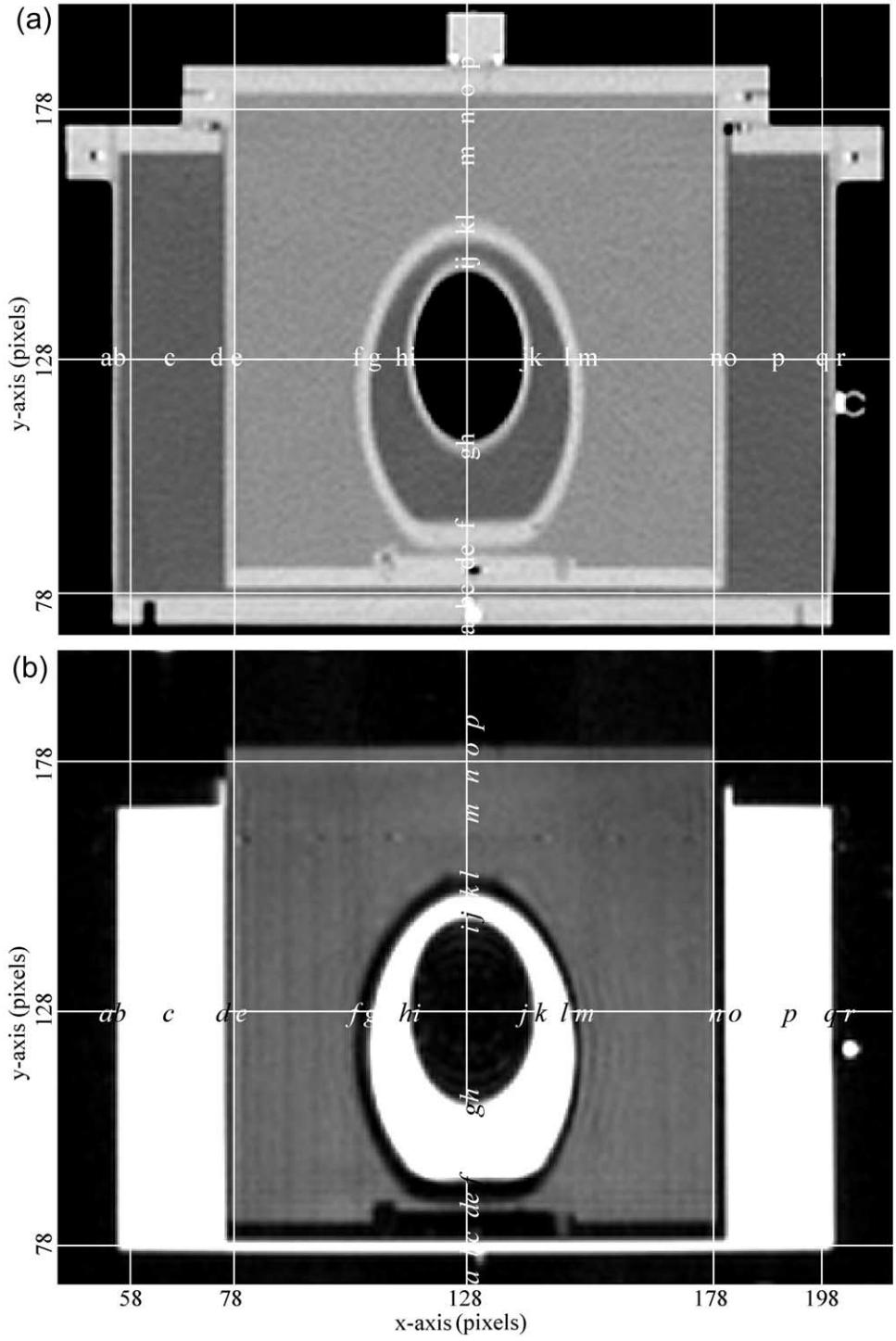

Fig. 3. (a) CT and (b) MR images (central slices) of the body phantom inside the reference frame. Perspex is seen as a high signal (almost white) in CT and no signal (black) in MR. Fat, water and air are seen to be dark grey, light grey and black, respectively, in CT and white and grey and black, respectively, in MR. The letters indicate the corresponding positions of voxel intensities studied between the CT and MR images of the phantom.

and FLASH 3D T1-weighted MR (TR = 18.8 ms, TE = 5 ms and bandwidth 244 Hz/pixel) were acquired using the same CT and MR scanners as in Section 2.2. The RT protocol involved scanning the patient supine in the treatment position 30 min after drinking approximately 500 ml of water in order to scan the patient with a full bladder. Identical flat couches with interlocking leg stocks, reference frame and internal lasers were used to aid reproducible patient positioning between the two imaging modalities and the treatment set-up. Tattoos produced as a part of radiotherapy planning procedure in CT were used to locate the pubic symphysis to position the patients using the lasers and reference frame

Table 1
Estimated prostate cancer patient set-up and imaging times for (a) conventional CT treatment planning scans (scans currently used for radiation treatment plans) and (b) CT and MRI comparison study[a]

	Time (min)
(a) Conventional CT treatment planning scans	
Position, straighten patient on flat couch using leg stocks Place radio-opaque markers on skin to locate symphysis Scout view to check the position of patient and markers Adjust patient or markers using lasers and info. from scout view	5–10
Move couch to start position	
Scan patient	12–15
Tattoo patient	1
Total	Approx. 20
(b) CT + MR treatment planning scans for comparison study	
CT	
Position, straighten patient using flat couch and interlocking leg stocks Place radio-opaque markers on skin to locate symphysis Scout view to check the position of patient and markers Adjust patient or markers using lasers and info. from scout view Align patient and centre of reference frame Check feet-to-frame distance	10–15
Move couch to start position	
Scan patient	15
Tattoo patient	1
MR	
Position, straighten patient using flat couch and interlocking leg stocks Align patient to lasers and centre of reference frame Check feet-to-frame distance	10
Move couch to start position	
Scan patient	10
Total	Approx. 50

[a] The times vary slightly from patient to patient.

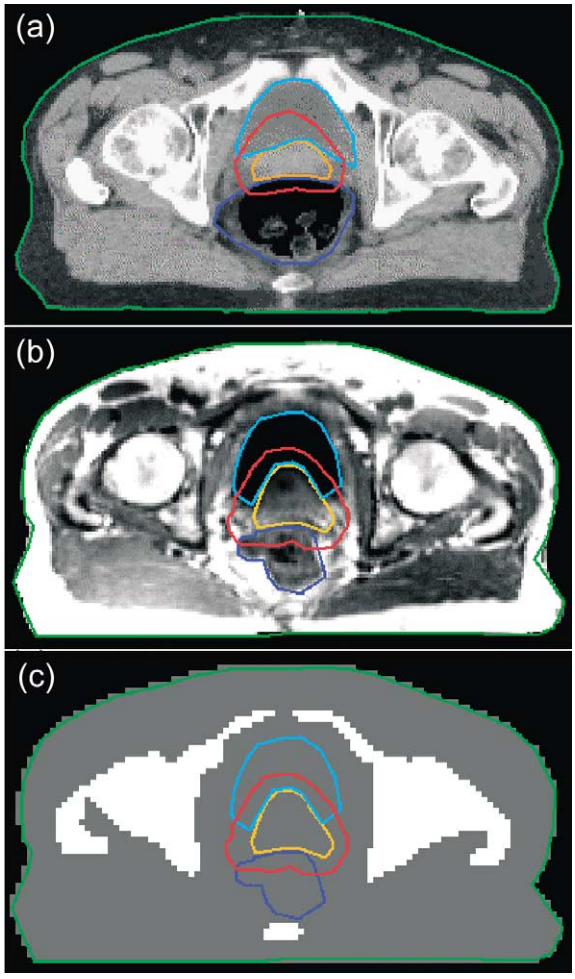

Fig. 4. Transverse slices for patient 5 of (a) CT and contours (b) MR and contours (c) and CT number bulk-assigned MR with contours. GTV is shown in orange, PTV in red, rectum in dark blue and bladder in light blue. Body outline is shown in light green. The outlines on MR were transferred onto the bulk-assigned MR.

in MR. Care was taken in repositioning the patient for each scan to minimise the amount of manual image registration required. Table 1a shows the conventional planning CT scan stages and the range of the approximate times. Table 1b shows the range of times approximated for different stages for the acquisition of the CT and MR scans for this study. Both scans had a slice thickness of 5 mm and were acquired with a matrix size of 256×256. All images included the whole bladder and rectum. CT and MR images of the patients were manually registered with six (three rotational and three translational) degrees of freedom using anatomical landmarks. This was achieved with an image-based manual registration, an in-house software. MR images were interpolated to match the CT resolution. The pixel size of the registered images was 1.95 mm.

The GTV and OARs (rectum and bladder) were outlined for CT and MR (Fig. 4a,b) for treatment planning. A single radiotherapy oncologist (MB) outlined all the images to avoid inter-observer variability. He was blinded to the images from the other modality when creating outlines. A uniform 1-cm 3D margin was added to the GTV to construct the PTV. The volumes of the structures from both CT and MR were measured and a paired *t*-test was conducted. The centre of mass of the GTV delineated from MR was measured and compared to the centre of mass determined from the GTV delineated from CT.

A separate outline was made on MR of the bony anatomy for bulk-density assignment. CRT treatment plans using three irregular fields, one anterior and two lateral wedged beams, with prescribed dose of 64 Gy to the PTV were created using VIRTUOS (DKFZ, Heidelberg, Germany) for CT + contours (Fig. 4a) and bulk-assigned MR + contours from MR (Fig. 4c). The latter image and contours will be referred to as MR and MR contours. Dose distributions were calculated for each plan. The treatment plans were then compared using the criterion (i.e. the protocol followed at the Royal Marsden Hospital for CRT planning) that the PTV receives dose between 93 and 107% dose normalised to the isocentre.

Table 2
Root mean square differences in Gy between dose distributions calculated on CT and I_{water}, and CT and $I_{bone+water}$ for the 60, 70, 80 and 90% isodose regions using Eq. (1)[a]

Patient number	$rms_{(D_{CT}-D_{water})}$(Gy)	$rms_{(D_{CT}-D_{bone+water})}$(Gy)
Voxels compared inside 60% isodose		
1	1.16	0.87
2	1.23	0.60
3	1.02	0.72
4	1.19	0.65
Voxels compared inside 70% isodose		
1	1.20	0.88
2	1.33	0.61
3	0.95	0.70
4	1.15	0.67
Voxels compared inside 80% isodose		
1	1.22	0.84
2	1.36	0.63
3	0.87	0.74
4	1.18	0.67
Voxels compared inside 90% isodose		
1	1.24	0.79
2	1.35	0.66
3	0.78	0.74
4	1.16	0.71

[a] All the rms values are greater for CT vs. I_{water} compared to CT vs. $I_{bone+water}$ indicating that the dose distribution observed in $I_{bone+water}$ is more similar to CT dose distribution.

3. Results

3.1. Validity of CT number bulk-assignment

Table 2 lists the rms dose differences that were calculated for isodose regions 60, 70, 80 and 90%. Lower isodose regions were also studied (smaller than 60% isodose). However, for these low dose regions, the rms values were too small to evaluate due to the small rms differences observed in low dose regions. The rms value between dose voxels from CT and I_{water} was always greater than that between CT and $I_{bone+water}$.

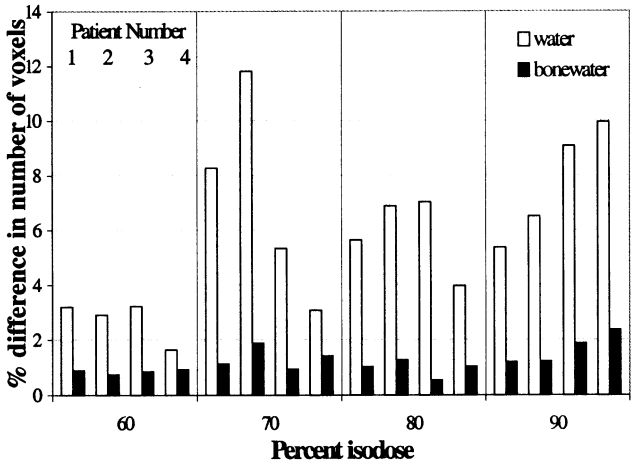

Fig. 5. Histogram of the percent difference of number of voxels inside the specified isodose regions compared between I_{water} and CT, and $I_{bone+water}$ and CT for four patient data. The percent differences of the number of voxels observed between I_{water} and CT were always greater than the percent differences observed between $I_{bone+water}$ and CT. The percent differences observed between $I_{bone+water}$ and CT were always less than 3% whereas for I_{water} and CT they were always greater than 3% and the maximum value was 12%.

The rms values for all patients were less than 1.36 Gy, only just over 2% change of the 64 Gy prescribed dose. The $rms_{(D_{CT}-D_{bone+water})}$ values were always less than $rms_{(D_{CT}-D_{water})}$. The difference between the two rms values for patient 3 (0.78 Gy for CT vs. I_{water} compared to 0.74 Gy for CT vs. $I_{bone+water}$) was not great for voxels compared inside the 90% isodose. However, as lower isodose volumes were studied, the difference became greater. This is seen as 1.02 Gy for CT vs. I_{water} compared to 0.72 Gy for CT vs. $I_{bone+water}$ as shown by voxels compared inside the 60% isodose for patient 3. For this patient, the dose delivered to the PTV is not be greatly affected by homogeneous electron-density bulk-assignment, but the dose to the OAR. which are concerned with doses greater than 50% say, may be more affected.

The number of voxels inside the isodoses 60, 70, 80 and 90% from the two bulk-assigned images were compared to CT and are plotted in Fig. 5. All four patient data are recorded for all isodose regions. For all $I_{bone+water}$ cases when compared with CT doses, the percent differences between the number of voxels were less than 2%. For I_{water}, however, the differences were always greater than 2% and

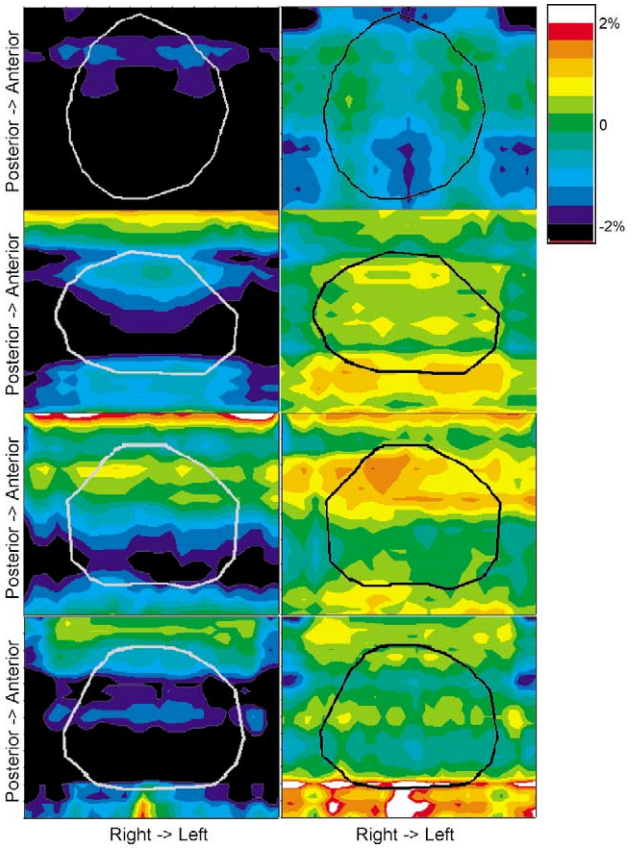

Fig. 6. Plot of Eq. (2) as topographic maps for CT vs. I_{water} (left column) and CT vs. $I_{bone+water}$ (right column) dose voxels for the central transverse slices from all four patients. Top and left of figures correspond to anterior and right side of the patient, respectively. Only the high-dose regions are plotted and the PTVs of the four patients are outlined in grey (left) or black (right). x- and y-axes indicate position within the 128×128 dose distribution matrix and each voxel size is $3.9 \times 3.9 \times 5.0$ mm^3. Black and white parts of the image indicate percent difference greater than 2% and green indicates no difference. The positive percent difference indicates that the CT-derived dose voxel was higher than the dose voxel derived from the bulk-assigned image. In general, the left column of maps indicates a larger difference inside the PTVs than the right images. The differences observed in the left column of maps indicate that D_{water} was generally greater than D_{CT}. On the other hand, the differences observed in the right column of maps indicate that the $D_{bone+water}$ was generally less than D_{CT}.

as great as 12%. This indicates that segmentation of bone and water gives a more accurate dose calculation than bulk-density assignment to water alone.

Although assessment of the rms value and comparing the number of voxels inside the dose regions were useful in assessing the global differences in dose, these parameters lack spatial information. Therefore, the doses were also compared using dose-difference maps, which were zoomed to show the high-dose regions (Fig. 6). The top of each figure corresponds to the anterior side of the patient and the left of the figure corresponds to the right side of the patient. Only the central slices containing the isocentre of the PTV (oval shapes in Fig. 6) from all four patients are presented in Fig. 6.

The differences between D_{CT} and D_{water} inside the PTV

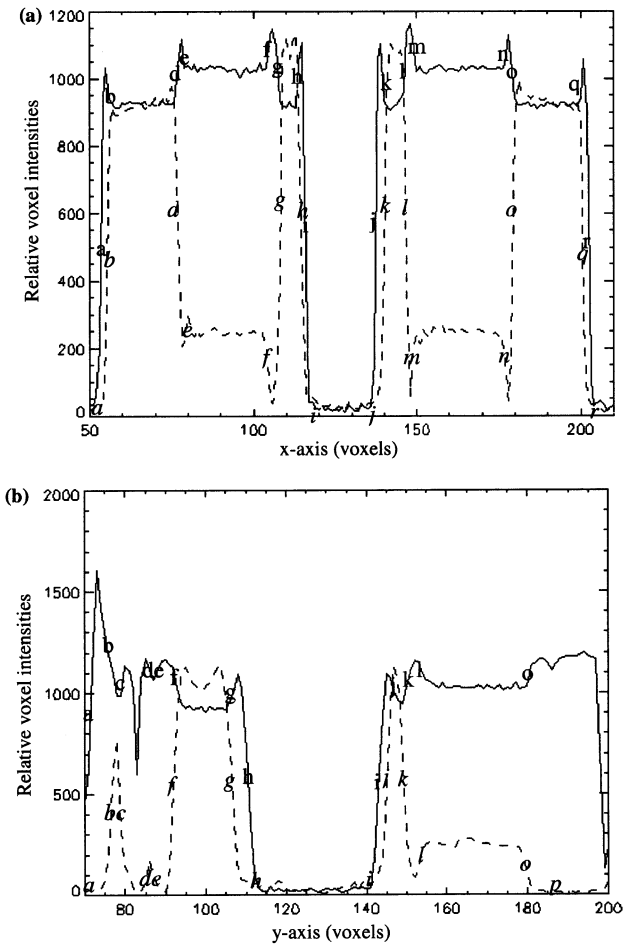

Fig. 7. Voxel intensities plotted for the lines in Fig. 3. (a) x-direction at $y = 128$ and (b) y-direction at $x = 128$. CT voxel intensities are represented in solid lines and MR voxel intensities are in broken lines. The letters correspond to those in Fig. 3. The positions in CT are shown in bold and in MR are shown in italicised letters.

were mostly greater than 2% as shown by the black regions in the left maps in Fig. 6. Differences ranged from an absolute percent difference of 0–5% in the high-dose regions. The dose distribution for I_{water} was in almost all cases higher than the dose distribution observed in CT inside the high-dose regions as shown by the negative percentage difference. This is presented as blue and black in the left column of images in Fig. 6. Differences greater than 2% (range 0–5%) were observed in the posterior and lateral PTV regions. Small or no differences were observed in the anterior regions of the PTV. There are some white regions (greater than 2%) visible in anterior regions of the dose maps for patient 3. The difference was considered insignificant since the doses in these regions were less than 30% of the prescribed dose. Thus, even a very small dose difference would show a large percent difference of dose.

The differences observed between D_{CT} and $D_{bone+water}$ inside PTV (Fig. 6, right column of maps) were less than 2% with the exception of the fourth patient. The central slice illustrating this is shown in Fig. 6d. This was up to a 2.7%

dose difference in the posterior region of the PTV but it was only observed in a small number of voxels (approx. three voxels, equivalent to 75 mm^3). The doses observed in $I_{bone+water}$ were always less than the dose observed in CT (shown as yellow and red in the dose difference maps on the right column in Fig. 6). One exception was seen in patient 1, where anterior and posterior regions of the PTV in $I_{bone+water}$ received a dose 1.2–1.6% more than the dose to CT. Overall, most of the high-dose regions in $I_{bone+water}$ received a dose less than 2% different from the dose distribution in CT.

3.2. Quantification of distortion

Fig. 7 shows the voxel intensities plotted for the corresponding central lines shown in Fig. 3. The positions shown in Fig. 3 are shown in Fig. 7. When the profiles in Fig. 7 are compared, while guided by the phantom images from Fig. 3, the different edges of the phantom imaged in CT and MR match up well in both *x*- and *y*-directions. This observation was made throughout all the profiles made for *x*- and *y*-axes at different slices. It should be noted that the solid and dashed lines in Fig. 7 do not match up exactly on top of each other. This is due to the intrinsic differences in signal observed for the two imaging modalities and is not due to distortion. For example, the high perspex signal of CT matches the null signal of MR (e.g. a to b), low oil signal on CT matches the high signal on MR (e.g. b to d in *x*-direction) and medium water signal matches low signal on MR (e.g. e to f in *x*-direction).

Fig. 8a shows the comparison between distances measured in the central slice between the letters as shown in CT (Fig. 3a) and MR (Fig. 3b) images of the phantom. Most of the distances lie on the unity curve. The deviations observed in the central slice were in the region of one pixel (1.95 mm). The average deviation observed in the central slice was 1.30 mm (maximum 3.80 mm) with S.D. of 1.04 mm. Fig. 8b shows the measurements obtained from the slices 35 mm inferior and superior from the central slice. The average deviation observed in these slices was 1.31 mm (maximum 5.00 mm) with a S.D. of 1.06 mm. Fig. 8c shows the measurements from the slices 70 mm inferior and 65 mm superior of the central slice. The average deviation observed was 1.94 mm (maximum 6.70 mm) with S.D. of 1.36 mm, still only about one pixel. The maximum deviation observed was on the *x*-axis from *b* to *q*, i.e. over a distance greater than 250 mm (see Fig. 3).

The magnitude of the distortions caused by deviations from a uniform magnetic field strength in an individual patient was estimated to be in the order of 1–3 mm. This estimation was made by effectively subtracting an image obtained using a gradient of one polarity from that produced using a gradient of the reverse polarity. The resulting shift of structures (divided by 2) observed using forward and reverse polarity gradients gives an estimation of the geometric distortions caused by deviations from a uniform magnetic field strength (i.e. patient based chemical shift/susceptibility and scanner based field inhomogeneities).

3.3. CT vs. MR prostate treatment planning

Fig. 9 compares the volumes delineated in all five patient CT and MR pelvic images. As seen in Fig. 9a, body volumes for CT and MR images were comparable. MR-derived volume was slightly smaller, however, the difference was only weakly significant ($P = 0.07$) since volumes of patient 4 were 5% different.

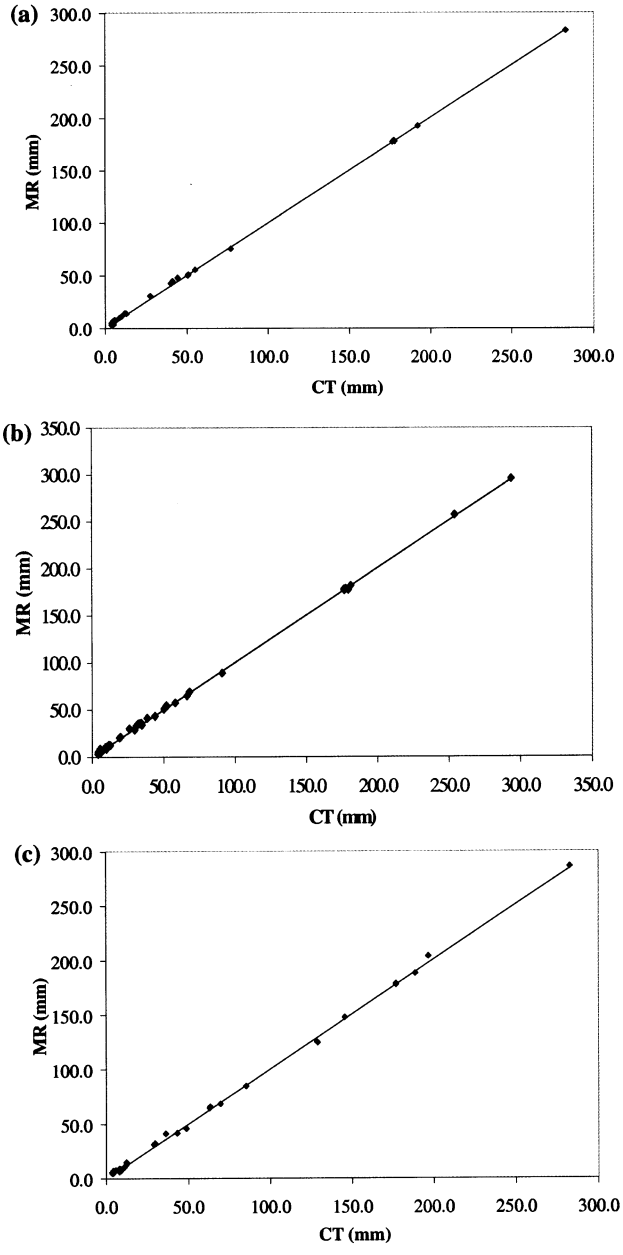

Fig. 8. Distances between positions indicated by letters in Fig. 3a for CT and MR were plotted against each other. The points are mostly on the line of unity. Slices at (a) 0 mm, (b) 35 mm and (c) 70 mm from the central slice are presented.

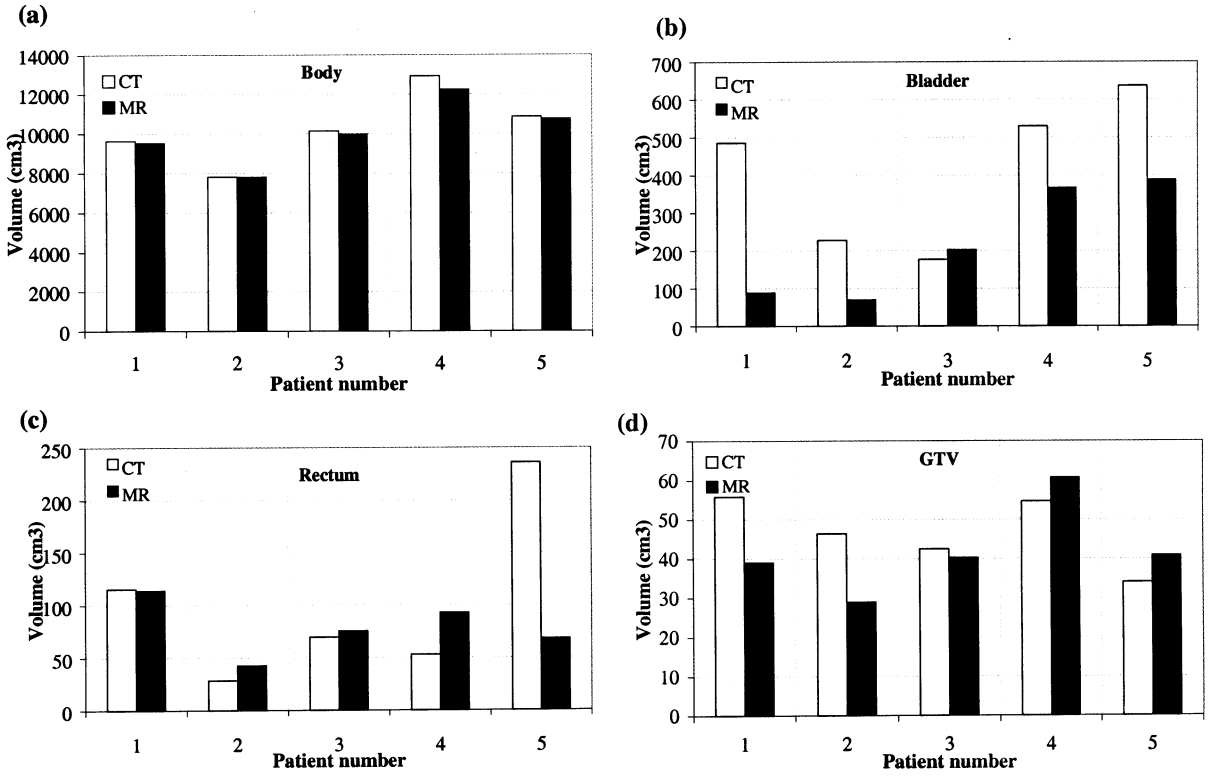

Fig. 9. Comparison between CT and MR (a) body volumes, (b) bladder volumes, (c) rectum volumes and (d) GTVs for five patients.

The bladder volumes, as shown in Fig. 9b, were dissimilar in all five patients ($P = 0.03$). In general, the CT-derived bladder volumes were larger than MR-derived bladder volumes with one exception where the volumes of the CT and the MR bladder were seen to be similar (patient 3). As a normal radiotherapy treatment protocol, prostate was treated with a full bladder. The first two patient MR-derived bladder volumes suggest that the bladder fillings have been difficult to control. The CT-derived bladder was more than five times the MR-derived bladder for the first patient (485.7 and 89.1 cm^3, respectively). Similarly, the CT-derived bladder was approximately three times larger than the MR-derived bladder in the second patient (227.9 and 69.8 cm^3, respectively). A comparison of rectal volumes as derived from CT and MR images for all five patients showed that they were dissimilar but this was not entirely unexpected since there was no protocol to keep the rectum the same size between the two scans. GTVs delineated from CT and MR do not follow any specific trend as shown in Fig. 9d. Table 3 lists the difference in positions observed in the left–right, anterior–posterior and inferior–superior between the centre of mass of the GTV as delineated by CT and MR. No pattern was observed for the five patients. All the lateral positional differences observed for centre of masses were smaller than 4 mm. However, in the anterior–posterior direction, the centre of mass of MR delineated GTV for one patient was 13.3 mm anterior to that of CT and for another MR, GTV was 14.8 mm posterior to the CT. No correlation was observed between the positional changes and bladder and rectal fillings for the five patients.

Table 3
Change in centre of mass (COM) of MR GTV from CT GTV in lateral, anterior–posterior and superior–inferior directions

Patient no.	Left–right (mm)	Anterior–posterior (mm)	Inferior–superior (mm)
1	4.2	13.3	0
2	0.1	2.0	2.5
3	0.1	1.7	− 7.5
4	− 0.6	− 14.8	0
5	− 0.7	− 1.9	5.0

Positive number indicates that MR COM is left, anterior and inferior compared to the CT COM.

Fig. 10 shows the results from treatment planning. In Fig. 10a, all the data above the black line indicate the fraction of the PTV receiving greater than 105% dose for all five patients. Both CT and MR dose-plans for all patients have small volumes receiving greater than 105% dose. Less than 3% of all PTVs received a greater than 105% dose. Table 4 shows the dose statistics for PTV calculated from 1% dose bins. All the volumes were receiving less than 107% dose.

Under the black line in Fig. 10a are the data for percent of PTVs receiving less than 95% dose. For all patients, the percent of PTVs delineated from CT and MR receiving less than 95% dose were different except for patient 4

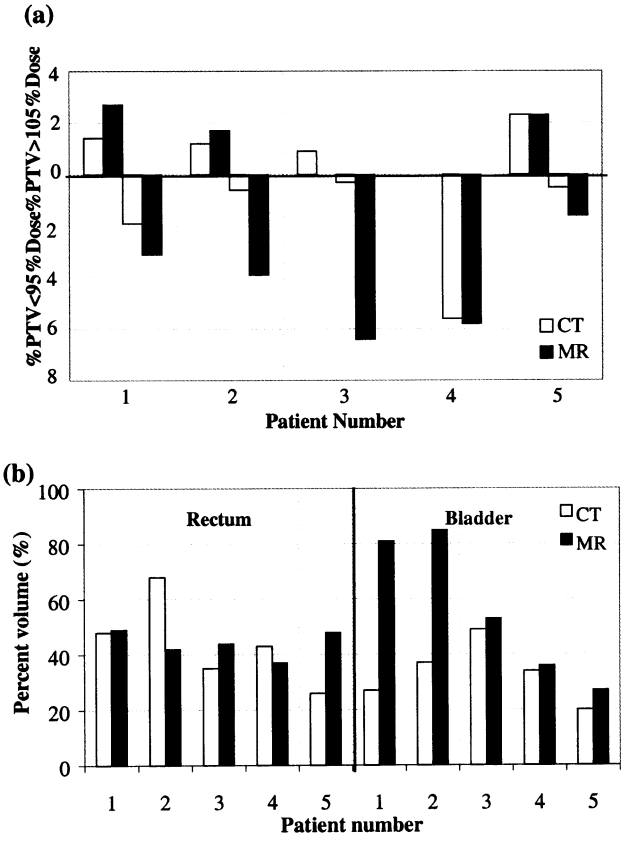

Fig. 10. (a) Percent of normalised planning target volumes receiving less than 95% (below the black line) or greater than 105% (above the black line) dose normalised to the isocentre for all five patient plans using CT and MR. All volumes met the criteria of being under 107% and greater than 95% of the prescribed dose. (b) Normalised organs-at-risk (rectum left, bladder right) volumes receiving greater than 50% dose normalised to the isocentre for all five patient plans using CT and MR. All were comparable except the first two patient bladder volumes where a much larger percent volumes received greater than 50% dose. This was attributed to smaller filling of the bladder prior to MR imaging as shown in Fig. 9b.

where 5.6% of CT-derived PTVs receive less than 95% dose compared to 5.8% of MR-derived PTVs. The worst case was patient 3, where 0.3% of CT-derived PTV received less than 95% dose and 6.4% of MR-derived PTV received less than 95% dose. However, all the plans were acceptable as the minimum dose seen in all the plans was greater than 93% of the normalised dose. Both CT and MR plans met the CRT planning criterion.

Fig. 10b shows both rectum and bladder volumes receiving greater than 50% dose normalised to the isocentre. The percent rectal volumes receiving greater than 50% dose is comparable in both CT and MR plans. The mean dose normalised to the isocentre for rectums, delineated in CT and MR, is shown in Table 4.

For three patients, specifically patients 3, 4 and 5, bladder volumes delineated from CT and MR receiving greater than 50% normalised to the isocentre are also comparable. However, for patients 1 and 2, most of the MR bladder receives greater than 50% dose (81 and 85%, respectively). The difference between the doses to the bladder delineated from the two modalities can also be seen by the mean dose in Table 4 (74.0, 74.7% MR compared to that of 28.7, 39.7% in CT). This was probably due to a small degree of bladder filling as was seen in Fig. 9b. If the bladder had been more full, the volume receiving greater than the specified dose would not have been so high.

4. Discussion

4.1. Validity of CT number bulk-assignment

The two bulk-density assigned plans were compared to the CT plan. Assigning a homogeneous density of water, greater than 2% difference in dose was noted in the high-dose regions when compared to the CT dose distribution. When bone was segmented and assigned an 'average bone' CT number (320 HU), the dose differed by less than 2% from the dose calculated using the full CT information. Therefore, when bone is segmented from a MR image and bone and water CT numbers are assigned to the MR, it is possible to use these adjusted data similarly to that of CT for RT treatment planning for prostate cancer.

Though the results consistently show that bone + water-assigned images produce a more similar dose distribution to CT than that of the water assigned image, the data sample is small and more detailed investigation would be required before clinical implementation.

4.2. Quantification of distortion

The effect of geometric distortion was negligible using the FLASH 3D MR sequence when measurements between CT and MR images of the phantom were compared to values found from registered CT images. Near the centre of the FOV, deviations of measurements in MR were about one

Table 4
Minimum, maximum and mean doses normalised to the isocentre delivered to the PTV, rectum and bladder delineated in CT and MR for the five prostate cancer patients

Patient no.	PTV			Rectum		Bladder	
	Min	Max	Mean	Max	Mean	Max	Mean
CT							
1	95.4	105.0	99.6	99.7	51.7	102.9	28.7
2	96.3	104.8	100.0	101.6	72.8	104.8	39.7
3	96.4	104.9	100.5	100.6	46.9	104.9	49.2
4	94.3	102.6	98.8	98.4	53.5	102.6	31.3
5	96.8	106.5	99.6	106.5	41.6	102.2	20.9
MR							
1	94.9	105.5	99.7	99.1	59.7	103.4	74.0
2	94.7	105.3	99.3	97.9	49.0	104.3	74.7
3	93.5	101.7	98.4	99.7	53.7	100.7	48.5
4	94.2	103.7	99.0	98.4	46.9	102.6	33.7
5	94.5	106.3	99.6	99.9	54.9	103.1	28.3

pixel compared to that of CT. In the slices 70 mm from the central transverse slice, the distortions were greater; up to 6.7 mm of deviation was observed in the lateral direction, i.e. *x*-axis direction. However, the average distortion was still about one pixel (1.95 mm). An inherent imaging uncertainty of 0.5 pixels is expected as the pixel represents some averaging of real space over its volume. The average distortion was deemed acceptable since the PTV localisation will not extend further than approximately 4 cm from the centre of the image. OARs and the body outlines may be more affected. However, the distortions will not be detrimental to treatment since distortion will not play a greater role than the OAR motion, which have been recorded to contribute ±30% in bladder and rectal volume changes [18]. Distortion increases with radial distance from the centre. However, in the central slice, the distortion is minimal even near the points near the skin surface. This can be seen by the letters b and q from Fig. 7a, which extend a distance of 30 cm laterally from the centre and also from letter o from Fig. 7b, which is a point 20 cm anterior from the couch in the central slice. As the skin surface markers are placed on the pubic symphysis, which is near where the central slice would be, the distortion is expected to be small. The phantom may be smaller than some large prostate cancer patients. However, the phantom results give an indication of the negligible distortion in the FLASH 3D sequence.

In agreement with Beavis et al., a large bandwidth MR sequence produces small geometrical distortions [1]. They used a receiver bandwidth of ±32 kHz similar to the bandwidth used to image the phantom ±31.2 kHz (equivalent to 244 Hz/pixel). Furthermore, we have used a sequence that uses phase encoding to read two directions of the image, which is less prone to geometrical distortions.

4.3. CT vs. MR prostate treatment planning

The CRT planning comparison of CT and bulk-assigned MR was conducted for illustrative purposes. Both treatment plans for all five patients were acceptable, as all of the PTV received doses greater than 93% and lower than 107%. Both CT- and MR- delineated rectum doses were acceptable as the volume of rectum receiving greater than 50% dose normalised to the isocentre were comparable. However, in the MR-delineated bladder of two patients, 80% of the bladder volume received greater than 50% dose. This was thought to be due to the small degree of bladder filling. The largest bladder differences were observed on the first two patients that were imaged. A more reproducible bladder filling was observed in the last three patients (percent difference between the CT to MR bladder volumes decreased from approx. 75 to 30%). This was attributed to the experience gained in patient set-up for this study. The goal of the volume comparisons was to show the difficulties in comparing images taken at two different times. An extensive volume comparison is beyond the scope of this study. The treatment planning results obtained in this study were not surprising since Sections 3.1 and 3.2 have shown that bone and water electron-density assigned images were adequate for calculating dose and the FLASH 3D sequence produces minimal geometrical distortion.

One of the reasons for not using MR alone for RT planning in the prostate is the lack of DRR's for use in verification. Further study is required to create prostate DRR using MR only but DRRs for brain have been shown in the literature [14,15,22]. The FLASH 3D sequence produced images with negligible distortion and comparable quality to CT. This imaging sequence can provide more accurate target volumes according to Khoo et al. [10]. They had conducted a qualitative test on the localisation of prostate on the four MR imaging sequences including FLASH 3D and CT. The 'five-point grading scale test' was based on segmentation ability of the prostatic apex, prostate, rectum, bladder and seminal vesicles for five patients by three observers. The FLASH 3D sequence scored the highest and was shown to provide improved definition of prostate treatment volumes. However, the images used had different slice thickness and image matrix sizes. Though all the other images had a 5-mm slice thickness, the FLASH 3D had a 1-mm slice thickness. The rationale behind choosing this slice thickness for this sequence was that all the other MR sequences do not contain contiguous information, which is present in FLASH 3D MR. Furthermore, the images were assessed using coronal and sagittal views as well as the axial view and since the slice thickness of FLASH 3D was very small, no degradation of the image would have been observed by displaying the images in different views. The images used in our study did not produce outlines of better quality since a slice thickness of 5 mm was used so that a simple, direct comparison could be made to CT. Furthermore, producing a 1-mm slice thickness would increase the imaging time, which is dependent on TR and number of slices ($t = \mathrm{TR} \times \mathrm{phase1} \times \mathrm{phase2}$ where phase1 is the matrix size of the *y* and phase2 is the number of slices). Therefore, by decreasing the slice thickness fivefold would increase the imaging time fivefold for the same volume.

The range of patient imaging times, including set-up, for our study was 20–30 min as shown in Table 1. The imaging times not including set-up in both CT and MR are only approximately 10 min. If MR were the only imaging modality, a different set-up protocol would be required due to the lack of a scoutview that is used to align the patient in CT. Moreover, the time required for set-up and imaging would also change. An outline of proposed times for set-up and imaging the patient in MR is shown in Table 5. The treatment planning times were not included in this table. With a single modality planning, there is no need for image registration so the planning time should decrease from that of multimodality treatment planning. However, bone segmentation is required for MR planning. This procedure currently takes 10 min for manual outlining, but more automatic methods could be employed in the future to reduce this workload.

Table 5
Proposed set-up and imaging time for MR scans for radiotherapy treatment planning of a prostate cancer patient

Proposed MR treatment planning scans	Time (min)
Pre-MRI simulator appointment Position, straighten patient on flat couch using leg stocks Mark and tattoo patient on skin to locate symphysis	10
Position, straighten patient on flat couch Adjust patient using lasers and information from simulator Move couch to start position	5–10
Scan patient	10
Total	Approx. 30

5. Conclusions

This study has shown that certain MR sequences can replace CT by proving the following techniques. As a full-density correction method does not exist for MRI, bulk-density assignment was tested. When CRT plans of prostate on bone + water density-assigned images were compared to the CT plans, dose distribution differences were negligible. The 'bone + water method' is a simple approximation to the full-density correction technique. Though the data sample was small, all four bone + water density assigned plans consistently produced negligible differences compared to CT plans whereas water-assigned plans did not. The distortion effects of FLASH 3D MR measured using a phantom averaged 2 mm and this has revealed that some MR imaging sequences will produce images with small distortions in sizeable volumes like the pelvis. Though FLASH 3D images used in this study may not be sufficient to replace CT in terms of better delineating the prostate, a methodology of using MR only for the use in CRT planning has been shown. MR sequences with small distortions or distortions that can be corrected can replace the role FLASH 3D sequence has played in this study [20]. This was a feasibility study to show that MR can be used instead of CT by bulk-assigning electron-density equivalent CT numbers and also by minimising distortion by using certain sequences. No attempt was made to optimise the MR sequence for the purpose of prostate planning in CRT.

A better contrast MR sequence using T2-weighted parameters is being researched. This sequence should have a large bandwidth to decrease the effects of distortion but have increased soft-tissue contrast in order to visualise the prostate better. The outcome of producing plans using two different image sets taken at different times, i.e. plans on two different outlines, for a single patient needs to be quantified. The GTV positional changes in MR from CT may be due to organ movements and not only due to the difficulty in delineation because of low soft-tissue contrast. The benefits of using only MR instead of CT and MR to delineate GTV for prostate CRT planning are increased imaging efficiency from the use of a single modality with superior soft-tissue contrast and reduced cost of treating each patient since only one imaging modality would be used for delineating the tumour. Though the doses to patient from CT scans are minimal, multiple scanning has become more common to reduce systematic errors and the dose should then also be considered. MR eliminates the concern.

Acknowledgements

We would like to thank David Dearnaley and Stephen Breen for their help in the completion of this paper and we are grateful for the support of Cancer Research UK for the work of the Joint Department of Physics. The project studying the uses of multimodality imaging in radiation therapy treatment planning is supported by the Engineering and Physical Science Research Council (grant number GR/M60514 DN173). We would also like to thank the DKFZ-Heidelberg for their support and providing us with the VOXELPLAN treatment planning system.

References

[1] Beavis AW, Gibbs P, Dealey RA, Whitton VJ. Radiotherapy treatment planning of brain tumours using MRI alone. Br J Radiol 1998;71:544–548.
[2] Bortfeld T, Schlegel W, Rhein B. Decomposition of pencil beam kernels for fast dose calculations in three-dimensional treatment planning. Med Phys 1993;20:311–318.
[3] Cancer Research Campaign. Scientific Yearbook 2000–2002. 2001 Cancer Research Campaign, 2002.
[4] Debois M, Oyen R, Maes F, Verswijvel G, Gatti G, Bosmans H, Feron M, Bellon E, Kutcher GJ, Van Poppel H, Vanuytsel L. The contribution of magnetic resonance imaging to the three-dimensional treatment planning of localized prostate cancer. Int J Radiat Oncol Biol Phys 1999;45:857–865.
[5] EUCAN. Cancer Incidence, Mortality and Prevalence in the European Union 1996 estimates), 1996.
[6] Fiorino C, Reni M, Bolognesi A, Cattaneo GM, Calandrino R. Intra- and inter-observer variability in contouring prostate and seminal vesicles: implications for conformal treatment planning. Radiother Oncol 1998;47:285–292.
[7] Gademann G, Schlegel W, Debus J, Schad L, Bortfeld T, Hover KH, Lorenz WJ, Wannenmacher M. Fractionated stereotactically guided radiotherapy of head and neck tumors: a report on clinical use of a new system in 195 cases. Radiother Oncol 1993;29:205–213.
[8] ICRU. ICRU Report 42: Use of computers in external beam radiotherapy procedures with high-energy photons and electrons. 1987. Maryland, USA, International Commission on Radiation Units and Measurements.
[9] ICRU. ICRU Report 46: Photon, electron, proton and neutron interaction data for body tissues. 1992. Maryland, USA, International Commission on Radiation Units and Measurements.
[10] Khoo VS, Padhani AR, Tanner SF, Finnigan DJ, Leach MO, Dearnaley DP. Comparison of MRI with CT for the radiotherapy planning of prostate cancer: a feasibility study. Br J Radiol 1999;72:590–597.
[11] McKenzie AL, van Herk M, Mijnheer B. The width of margins in radiotherapy treatment plans. Phys Med Biol 2000;45:3331–3342.
[12] Mizowaki T, Nagata Y, Okajima K, Kokubo M, Negoro Y, Araki N, Hiraoka M. Reproducibility of geometric distortion in magnetic resonance imaging based on phantom studies. Radiother Oncol 2000;57:237–242.
[13] Nutting CM, Khoo VS, Walker V, McNair H, Beardmore C, Norman

A, Dearnaley DP. A randomized study of the use of a customized immobilization system in the treatment of prostate cancer with conformal radiotherapy. Radiother Oncol 2000;54:1–9.

[14] Ramsey CR, Arwood D, Scaperoth D, Oliver AL. Clinical application of digitally-reconstructed radiographs generated from magnetic resonance imaging for intracranial lesions. Int J Radiat Oncol Biol Phys 1999;45:797–802.

[15] Ramsey CR, Oliver AL. Magnetic resonance imaging based digitally reconstructed radiographs, virtual simulation, and three-dimensional treatment planning for brain neoplasms. Med Phys 1998;25:1928–1934.

[16] Rasch C, Barillot I, Remeijer P, Touw A, van Herk M, Lebesque JV. Definition of the prostate in CT and MRI: a multi-observer study. Int J Radiat Oncol Biol Phys 1999;43:57–66.

[17] Roach M, Faillace AP, Malfatti C, Holland J, Hricak H. Prostate volumes defined by magnetic resonance imaging and computerized tomographic scans for three-dimensional conformal radiotherapy. Int J Radiat Oncol Biol Phys 1996;35:1011–1018.

[18] Roeske JC, Forman JD, Mesina CF, He T, Pelizzari CA, Fontenla E, Vijayakumar S, Chen GT. Evaluation of changes in the size and location of the prostate, seminal vesicles, bladder, and rectum during a course of external beam radiation therapy. Int J Radiat Oncol Biol Phys 1995;33:1321–1329.

[19] Seddon B, Bidmead M, Wilson J, Khoo V, Dearnaley D. Target volume definition in conformal radiotherapy for prostate cancer: quality assurance in the MRC RT-01 trial. Radiother Oncol 2000;56:73–83.

[20] Tanner SF, Finnigan DJ, Khoo VS, Mayles P, Dearnaley DP, Leach MO. Radiotherapy planning of the pelvis using distortion corrected MR images: the removal of system distortions. Phys Med Biol 2000;45:2117–2132.

[21] van Herk M, Remeijer P, Rasch C, Lebesque JV. The probability of correct target dosage: dose-population histograms for deriving treatment margins in radiotherapy. Int J Radiat Oncol Biol Phys 2000;47:1121–1135.

[22] Yin FF, Gao Q, Xie H, Nelson DF, Yu Y, Kwok WE, Totterman S, Schell MC, Rubin P. MR image-guided portal verification for brain treatment field. Int J Radiat Oncol Biol Phys 1998;40:703–711.